J. Membrane Biol. 194, 165–176 (2003)
DOI: 10.1007/s00232-003-2033-9

The Journal of
Membrane
Biology

Regulation of Ion Fluxes, Cell Volume and Gap Junctional Coupling by cGMP in GFSHR-17 Granulosa Cells

A. Ngezahayo, B. Altmann, H.-A. Kolb
Institut für Biophysik, Universität Hannover, Herrenhäuserstr. 2, D-30419 Hannover, Germany

Received: 31 December 2002/Revised: 17 April 2003

Abstract. Gap junctional communication between granulosa cells seems to play a crucial role for follicular growth and atresia. Application of the double whole-cell patch-clamp- and ratiometric fura-2-techniques allowed a simultaneous measurement of gap junctional conductance (G_j) and cytoplasmic concentration of free Ca^{2+} ($[Ca^{2+}]_i$) in a rat granulosa cell line GFSHR-17. The voltage-dependent gating of G_j varied for different cell pairs. One population exhibited a bell-shape dependence of G_j on transjunctional voltage, which was strikingly similar to that of Cx43/Cx43 homotypic gap junction channels expressed in pairs of oocytes of *Xenopus laevis*. Within 15–20 min, gap junctional uncoupling occurred spontaneously, which was preceded by a sustained increase of $[Ca^{2+}]_i$ and accompanied by shrinkage of cellular volume. These responses to the whole-cell configuration were avoided by absence of extracellular Ca^{2+}, blockage of K^+ efflux, or addition of 8-bromoguanosine 3′,5′-cyclic monophosphate (8-Br-cGMP) to the pipette solution. Even in the absence of extracellular Ca^{2+} or blockage of K^+ efflux, formation of whole-cell configuration generated a Ca^{2+} spike that could be suppressed by the presence of 8-Br-cGMP. We propose that intracellular cGMP regulates Ca^{2+} release from intracellular Ca^{2+} stores, which activates sustained Ca^{2+} influx, K^+ efflux and cellular shrinkage. We discuss whether gap junctional conductance is directly affected by cGMP or by cellular shrinkage and whether gap junctional coupling and/or cell shrinkage is involved in the regulation of apoptotic/necrotic processes in granulosa cells.

Correspondence to: H.-A. Kolb; email: kolb@mbox.biophysik.uni-hannover.de

Key words: Granulosa cells — Gap junctions — Ca^{2+} — Cell volume shrinkage — cGMP — Apoptosis

Introduction

Gap junctions are clusters of cell-cell channels that enable neighboring cells to exchange small signalling molecules (≤1 kDa) such as Ca^{2+}, cAMP, IP_3, and to propagate electric activities (Bruzzone, White & Paul, 1996; White & Paul, 1999; Harris, 2001). The gap junctional channels are composed of connexins, which are homologous proteins. So far, 19 and 20 connexin (Cx) genes have been found in the mouse and the human genome, respectively, that are specifically expressed and regulated in different cell types (Willecke et al., 2002). The connexins hexamerize and form connexons (hemichannels) that are inserted in the membrane of a single cell. The cell-cell channel is formed when hemichannels of two adjacent cells associate by their extracellular domains. Since in all tissues analyzed so far, at least two types of connexins are expressed (Bruzzone et al., 1996; White & Paul, 1999), connexons and gap junctional channels with complex stoichiometries can be expected. A connexon can be homomeric or heteromeric, depending on the presence of one or several connexin types, respectively. The gap junction channel formed by equally homomeric connexons is called homotypic. Two homomeric connexons composed of different connexin types build a heterotypic gap junctional channel and a cell-cell channel composed of two heteromeric connexons will be called heteromeric (Goodenough, Simon & Paul, 1999; White & Paul, 1999). Oocytes of *Xenopus laevis* have been very useful to characterize the regulation (e.g., gating by voltage) and the transport capacity of homotypic gap junctional channels. But the results obtained from

heterologous expression systems did not allow a reliable prediction of the properties of gap junctional channels composed of different connexin isoforms as expressed in original tissues (White & Bruzzone, 1996; Elenes et al., 2001).

The most abundant cells of the follicular system, the granulosa cells, express different connexins during their hormone-regulated proliferation and differentiation (Wright et al., 2001). The gap junctional channels in granulosa cells of rat are mainly composed of the phosphoprotein Cx43, though Cx45 is also expressed. During the follicular development, the expression pattern and posttranslational modifications, like phosphorylation of connexins, change (Schreiber et al., 1993; Okuma et al., 1995; Sommersberg et al., 2000; Wright et al., 2001). As demonstrated by Ackert et al. (2001), the gap junctional communication between the granulosa cells plays an important role in folliculogenesis. They showed that follicular growth could not be induced in Cx43-deficient mice. Furthermore, the induction of atresia, which corresponds to the elimination of granulosa cells through apoptotic/necrotic processes (Tilly, 1996), is concomitant with a reduced expression of Cx43 in rat granulosa cells (Wiesen & Midgley, 1994). It was therefore hypothesized that a loss of gap junctional communication contributes to the apoptotic processes during atresia. Despite the crucial role of gap junctional communication for follicular physiology and atresia, the regulation of gap junctional conductance between granulosa cells has not yet been studied. In order to understand the effects of gonadotropins and estrogens on the gap junctional communication of granulosa cells, hormonal effects on the conducting activity of the gap junctional channels have to be analyzed.

For the first time we quantitatively analyzed the voltage gating and intracellular regulation of gap junctional coupling of granulosa cells, using the cell line GFSHR-17. GFSHR-17 cells express the receptor for the follicular stimulating hormone (FSH). This cell line is considered to be suitable for analysis of the FSH-dependent maturation and as an in vitro cell model of granulosa cells (Keren et al., 1993; Sommersberg et al., 2000). We applied the double whole-cell patch-clamp technique in combination with a simultaneous measurement of $[Ca^{2+}]_i$. Establishing the double whole-cell configuration caused a spontaneously occurring gap junctional uncoupling in parallel with a sustained rise of $[Ca^{2+}]_i$ and cell shrinkage. These cellular reactions could be suppressed by blockage of K^+ efflux or by use of a nominally Ca^{2+}-free bath solution. Both modifications could be substituted by addition of 8-Br-cGMP to the pipette solution. The data indicate that cGMP depletion is related to Ca^{2+} entry and to K^+ release, which causes cell shrinkage and induces gap junctional uncoupling in granulosa cells.

Table 1. Composition of control bath and different pipette solutions

	Control bath solution [mM]	Pipette solution [mM]		
		A	B	C
NaCl	140	0	0	0
K-gluconate	0	100	100	100
KCl	5	40	0	40
CsCl	0	0	40	0
Na_2ATP	0	5	5	5
HEPES	10	10	10	10
Glucose	5	1	1	1
$CaCl_2$	1	0.1	0.1	0.1
$MgCl_2$	1	2.5	2.5	2.5
EGTA	0	0.4	0.4	0.4
8-Br-cGMP	0	0	0	0.05
pH	7.4	7.3	7.3	7.3

Materials and Methods

Cell Culture

Granulosa cell line GFSHR-17 (Keren et al., 1993) with passage number 5 was cultivated in petri dishes at 37°C under an atmosphere of 5% CO_2–95% air. Cells were fed with Dulbecco's F12 modified Eagle's medium (DMEM, pH 7.4, Sigma) supplemented with 10% fetal calf serum and penicillin and streptomycin. The culture medium was replaced every 3 days. After 7 days a cell monolayer was formed. Then the cells were trypsinized, collected and centrifuged for 5 min at $100 \times g$. The pellet was resuspended in 10 ml DMEM. For the measurements, 1–2 μl of the cell suspension were placed on a cover slip in a petri dish. After 5 min, the cells had adhered and 2–3 ml of culture medium were added to the dish. The cells were cultivated as described above and used for double whole-cell patch-clamp experiments 2–5 days later. Cells of passage number 6–10 were cryoconserved and used as stock. Cells were utilized up to a total of 25 passages.

Pipette Solutions

For composition and nomenclature of the different pipette solutions see Table 1.

Measurement of Gap Junctional Coupling and Cytoplasmic Free Calcium $[Ca^{2+}]_i$

Double Whole-cell Patch-clamp Analysis

A cover slip with cells was transferred to a superfusion chamber containing 0.5 ml bath solution. The chamber was mounted on a Zeiss inverted microscope (Oberkochen, Germany). The cells were washed with 10 ml (2 ml/min) of the bath solution and allowed to adapt to room temperature (~20°C) for at least 30 min. The double whole-cell patch-clamp configuration was established for an isolated cell pair according to Neyton & Trautmann (1985) (cf. Ngezahayo & Kolb, 1994; Fig. 1), using two patch-clamp amplifiers EPC 7 (List Medical, Darmstadt, Germany). The electrophysiological data were filtered at 3 kHz and digitized at 10 kHz via an

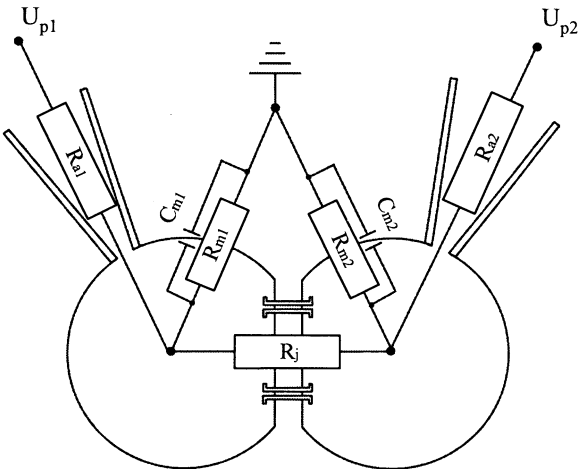

Fig. 1. Model circuit of the double whole-cell configuration of a cell pair coupled by gap junctional channels. U_{p1} and U_{p2} are the potentials of electrodes 1 and 2. Serial access resistances are given by R_{a1} and R_{a2}. Nonjunctional membrane resistances are denoted by R_{m1} and R_{m2}, respectively. R_j gives the gap junctional resistance. C_{m1} and C_{m2} represent the membrane capacities of the corresponding cells.

interface ITC 16 (Instrutech, Minnesota, USA). The data acquisition and off-line analysis were done using Pulse Pulsefit (HEKA Electronics, Lamprecht, Germany).

For measurement of the time course of gap junctional conductance (G_j), both cells were clamped to a holding potential of −40 mV near their resting potential U_m (generally between −30 to −38 mV), resulting in a net zero junctional current and a zero nonjunctional current. Thereafter, a voltage jump ΔU_p of ±10 mV was applied every 30 s for 100 ms to one cell, respectively. A model circuit of resistances for the double whole-cell configuration is given in Fig. 1. The serial resistances R_{a1}, R_{a2} varied between 5 and 12 MΩ for all pipette solutions (*see* Table 1). The non-gap junctional membrane resistance R_{m2} was in the range of 0.25 to 2.0 GΩ. To avoid significant errors in the determination of G_j, only experiments with $|R_{a1}-R_{a2}| < 1$ MΩ, $|R_{m1}-R_{m2}| < 25$ MΩ and $|U_{m1}-U_{m2}| < 1.5$ mV were considered (*see* Veenstra 2001). If the serial resistances R_{a1} and R_{a2}, the membrane resistances R_{m1} and R_{m2} and the membrane potentials U_{m1} and U_{m2} are not significantly different, G_j can be calculated using the equation:

$$G_j = \frac{-\Delta I_{p2} \cdot \left(1 + \frac{R_{a2}}{R_{m2}}\right)}{\Delta U_{p1} - R_{a1} \cdot \Delta I_{p1} + R_{a2} \cdot \Delta I_{p2}} \quad (1)$$

Index *1* denotes the cell at which a voltage jump from the common holding potential (−40 mV) was applied and index *2*, the other member of the cell pair, which was clamped to the holding potential. To analyze the voltage dependence of G_j, voltage pulses ΔU_{p1} between −120 and 120 mV were added to the holding potential of −40 mV, in steps of 10 mV with a duration of 1 s, and the evoked current responses I_{p1} and I_{p2} were recorded.

In some cell pairs (*see* Results), a voltage- and time-dependent current decrease was observed. To describe the voltage sensitivity of the corresponding gap junctional conductance, the steady-state conductance G_{ss} was calculated from the current values recorded during the last 50 ms of the applied pulse of 1 s. For clearer presentation, G_{ss} was normalized to the maximal value of G_j (G_{max}), which was derived as the mean initial conductance value (G_{inst}) recorded within 20 ms after application of a voltage pulse. G_{ss}/G_{max} values were plotted as function of ΔU_{p1} and fitted by a relation that describes the voltage dependence at both polarities (Chen-Izu, Moreno & Spangler, 2001)

$$G_{ss}/G_{max} = G_{min} + (G_{max} - G_{min})/ (1 + e^{(-\Delta U_{p1} - \Delta U_1)A_1})(1 + e^{(\Delta U_{p1} - \Delta U_2)A_2}) \quad (2)$$

to provide an estimation of ΔU_1 and ΔU_2, the voltages of half-activation for each of the connexons. A_1 and A_2 are the cooperativity factor describing the voltage dependence of the open-closed equilibrium for each of the connexons. G_{min} denotes the minimal value of G_j as function of ΔU_{p1}. Experiments were performed at room temperature. Data are given as mean ± SEM; *n* denotes the number of independent experiments (cell pairs).

Measurement of $[Ca^{2+}]_i$

Measurement of intracellular Ca^{2+} ($[Ca^{2+}]_i$) was performed according to Grynkiewicz, Poenie & Tsien (1985). To allow a measurement of $[Ca^{2+}]_i$ prior and after whole-cell patch formation, the cells were loaded with fura 2-AM (5 μM and 1% DMSO) (Molecular Probes) for 45–60 min at room temperature. The fura 2-AM-loaded cells were then transferred to a superfusion chamber, mounted onto an inverted microscope (*see* above). The cells were superfused with a bath solution (2 ml/min) for at least 5 min to wash out extracellular fura 2-AM and DMSO. The loaded cells were excited at 340 nm and 380 nm using a monochromator polychrome II (T.I.L.L. Photonics, Planegg, Germany) equipped with a 75 W XBO xenon lamp. To minimize the dilution of intracellular fura-2 concentration by the whole-cell formation, 50 μM K_5-fura-2 (Molecular Probes) were added to the pipette solution. This concentration of K_5-fura-2 was found to be suitable to obtain an about constant fluorescence signal at 340 nm and 380 nm prior and after whole-cell configuration. The fluorescence was registered with a digital CCD camera (C4742-95, Hamamatsu Photonics K.K.; Japan). The 340 nm to 380 nm excitation ratios of the fluorescence images were then calculated and calibrated to determine $[Ca^{2+}]i$, using the program Aquacosmos (Hamamatsu Photonics K.K.; Japan). The program was also used to estimate relative changes of cell diameters.

Results

Voltage Dependence of Gap Junctional Conductance

The double whole-cell patch-clamp configuration was applied to an isolated cell pair and both cells were clamped to a holding potential of −40 mV close to a membrane potential of −30 mV to −38 mV. To analyze the voltage dependence of G_j, one cell was clamped to test voltages (U_{p1}) of −160 mV to +80 mV in steps of 10 mV, applied for 1 s, while the holding potential of the adjacent cell was kept constant (*see* Fig. 1*A*, 1*B*). This allowed imposition of transjunctional voltages (ΔU_{p1}) of −120 mV to 120 mV.

Independently of the pipette solution, G_j varied as function of ΔU_{p1} for different cell pairs. 37 cell pairs out of a total of 60 cell pairs showed a voltage independence of voltage-jump current-relaxations as well as of G_j. Figure 2*C* and 2*D* show representative series of current relaxations of cell 1 (I_{p1}) and cell 2

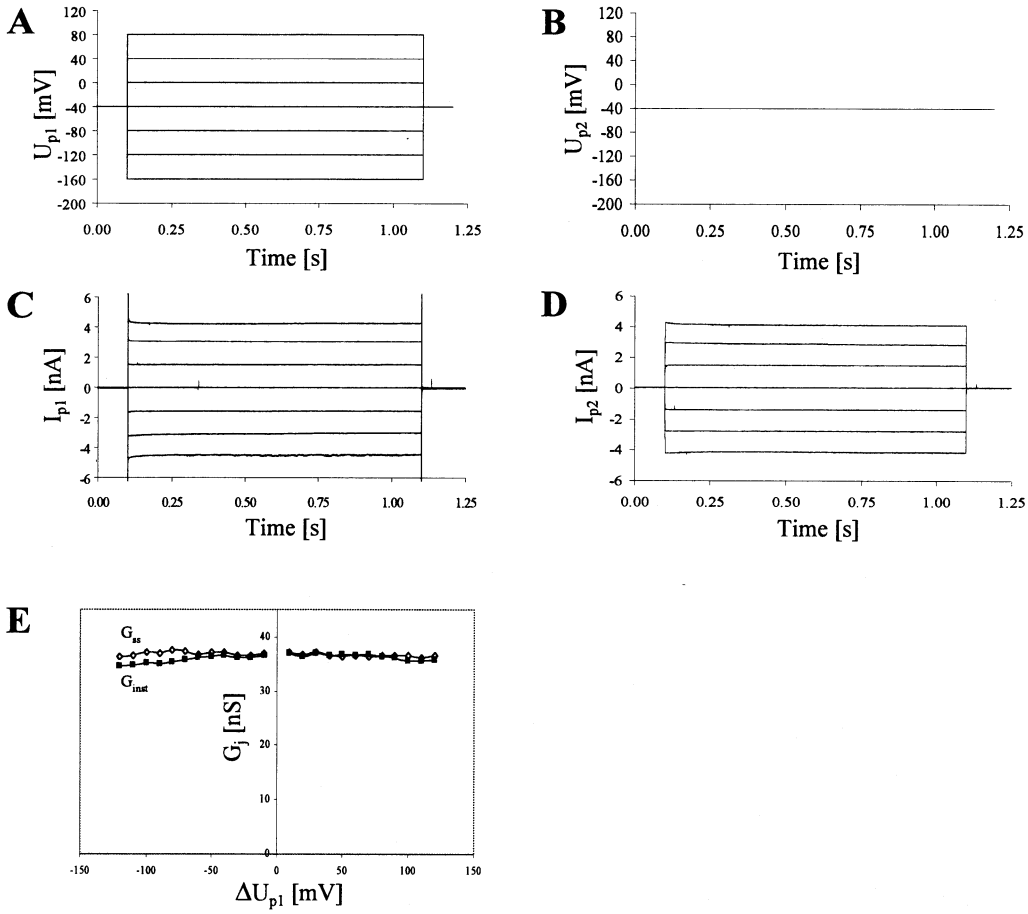

Fig. 2. Voltage protocol applied to cell 1 (U_{p1}) and cell 2 (U_{p2}), evoked currents (I_{p1}, I_{p2}) and gap junctional conductance (G_j). (*A*) Voltage steps applied to cell 1. (*B*) Cell 2 was clamped at the constant holding potential of −40 mV. (*C*) and (*D*) Current response of cell 1 and cell 2, respectively. (*E*) Gap junctional conductance (G_j) as function of ΔU_{p1}. The instantaneous gap junctional conductance (G_{inst}) was derived as mean value within the first 20 ms after application of a voltage step and the quasi-steady-state gap junctional conductance (G_{ss}), 50 ms before the voltage step of 1 s ended. For clearer presentation only the voltage steps to −160, −120, −80, −40, 0, 40, 80 mV (*A*) and the corresponding current responses (*C* and *D*) are presented. Control bath and pipette solution A (Table 1) were used.

(I_{p2}) in response to test voltages applied to cell 1. The current records indicate an almost voltage-independent behavior, which is reflected in the gap junctional conductance. Figure 2*E* presents the corresponding instantaneous gap junctional conductance (G_{inst}) and the quasi steady-state values of G_j (G_{ss}) as function of ΔU_{p1}, respectively; the two functions do not differ significantly in their amplitude.

A significant voltage-dependent inactivation of junctional currents was obtained for 9 cell pairs, which was observed in the range of -50 mV $> \Delta U_{p1} >$ 50 mV. Figure 3*A, B* shows representative current records in response to the voltage protocol given in Fig. 2*A, B*. The current relaxations of both cells decrease in a voltage- and time-dependent manner. The time course of the currents could be described by a sum of two exponential functions. The corresponding time constants τ_1 and τ_2 are given in Table 2. The corresponding gap junctional conductances G_{inst} and G_{ss} are presented in Fig. 3*C*. No significant voltage dependence of G_{inst} is observed, but G_{ss} exhibits a bell-shaped course as function of ΔU_{p1}, with a maximum in the range of -50 mV $> \Delta U_{p1} >$ 50 mV. For a more detailed analysis of the voltage dependence of G_j, the corresponding normalized conductance G_{ss}/G_{inst} was described by Eq. 2 (Materials and Methods). From a fit of Eq. 2 to the data (Fig. 3*D*), half-maximal inactivation voltages, according to the polarity of the applied voltage pulse, of $\Delta U_1 = -61.3 \pm 0.8$ mV and $\Delta U_2 = 66.4 \pm 1.0$ mV and for the corresponding voltage sensitivities $A_1 = 0.13 \pm 0.01$ mV^{-1} and $A_2 = 0.08 \pm 0.01$ mV^{-1} ($n = 9$) were derived.

In three cell pairs, the application of the voltage protocol given in Fig. 2*A*, 2*B* caused a time-dependent activation of the junctional current, which rapidly reached a stationary value within about 50 ms. Figure 4 shows the result of a representative experiment, which indicates a voltage-independent activation of current and conductance of the gap junctional channels.

In 11 cell pairs, a variable superposition of a voltage-dependent inactivating and voltage-

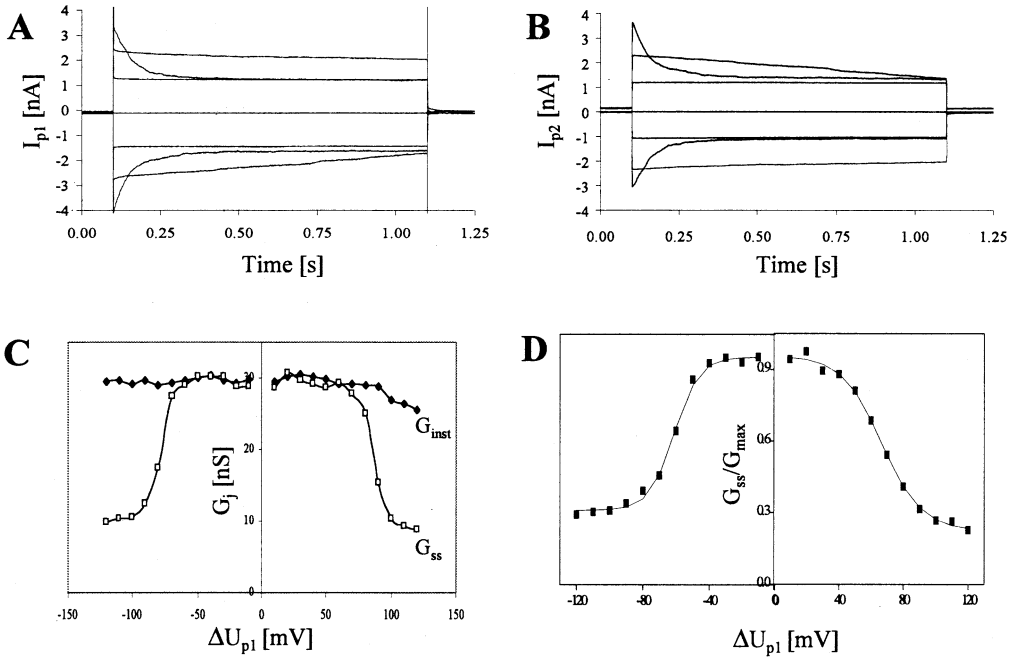

Fig. 3. Evoked currents and corresponding gap junctional conductance. (*A*) and (*B*) Current responses of electrode/pipette 1 and 2 after application of the voltage protocol given in Fig. 2*A*, *B*, respectively. (*C*) G_{inst} and G_{ss} as function of ΔU_{p1}. (*D*) G_{ss} as function of ΔU_{p1}, which was normalized to the maximal value of G_j (G_{max}). G_{max} was derived as the mean initial conductance value recorded within 20 ms after application of a voltage pulse ΔU_j. The mean values of G_{ss} were obtained from 9 different cell pairs. G_{ss}/G_{max} vs ΔU_j was fitted by Eq. 2. The result is given by the lines drawn. For further explanation, *see* Fig. 2 and text.

Table 2. Time constants of current inactivation τ_1, τ_2

ΔU_{p1} [mV]	τ_1 [ms]	τ_2 [ms]
−120	21.1 ± 4.6	184.4 ± 27.0
−110	31.6 ± 9.5	331.5 ± 13.5
−100	57.5 ± 20.6	1165.8 ± 244.0
−90	126.4 ± 48.3	2776.8 ± 505.6
−80	292.8 ± 93.7	6546.0 ± 1435.8
80	303.8 ± 36.6	6835.3 ± 1911.5
90	141.9 ± 18.9	2325.3 ± 956.6
100	86.7 ± 11.3	903.0 ± 47.4
110	43.0 ± 4.9	344.0 ± 19.7
120	16.6 ± 1.7	187.4 ± 31.4

Time constants τ_1 and τ_2 were measured after transjunctional voltage steps from a holding potential of −40 mV to test potentials (ΔUp_1) for $n = 9$ different cell pairs, respectively. The corresponding current inactivation $I(t)$ was fitted by a sum of two single-exponential functions given by: $I(t) = B_1 \cdot \exp(-t/\tau_1) + B_2 \cdot \exp(-t/\tau_2)$ + constant where B_1 and B_2 denote the corresponding current amplitude

independent activating behavior was observed (*data not shown*). A correlation of this finding with the specific passage number could not be found.

Time Course of $[Ca^{2+}]_i$, Cell Volume and G_j After Whole-cell Formation

Control Bath and Pipette Solution A

Using control bath and pipette solution A (*see* Table 1, additionally containing 50 μM K_5-fura-2), the time course of $[Ca^{2+}]_i$, cell volume and G_j could be followed on cell pairs after formation of the two consecutively performed whole-cell configurations that are necessary for establishing the double whole-cell formation (*see* Materials and Methods). A typical experiment is shown in Fig. 5. The formation of the first whole-cell configuration on cell 1 caused a rapid rise of $[Ca^{2+}]_i$ within less than a minute from a resting level of 65 ± 5 nM ($n = 20$) to values above 350 nM. It is interesting to note and will be considered in the Discussion that despite the known permeability of gap junctional channels for Ca^{2+} and a large initial value of G_{j0} of about 40 nS, the adjacent cell 2 responded in the time scale of several minutes by a far less pronounced increase of $[Ca^{2+}]_i$. (*see* Fig. 5*A* and Inset). Consecutive formation of the whole-cell configuration on cell 2 caused a rapid and steep rise of $[Ca^{2+}]_i$ in this cell, which is partially reflected in the neighboring cell. Thereafter the time course of G_j could be recorded, which is given in Fig. 5*B*. Comparison of Fig. 5*A* and 5*B* indicates that the rapid rise of $[Ca^{2+}]_i$ causes no significant change of G_j, but during the observed sustained increase of $[Ca^{2+}]_i$ the gap junctional conductance declines to about 1% of the initial value (G_{j0}) within 15–20 min. This finding was obtained also in the absence of recording $[Ca^{2+}]_i$. In parallel, cell shrinkage was observed (*see* Fig. 5*C*), which occurs at a similar time scale. For easier quantification of the cell size, single cells of spherical shape were selected and the cellular diameter was

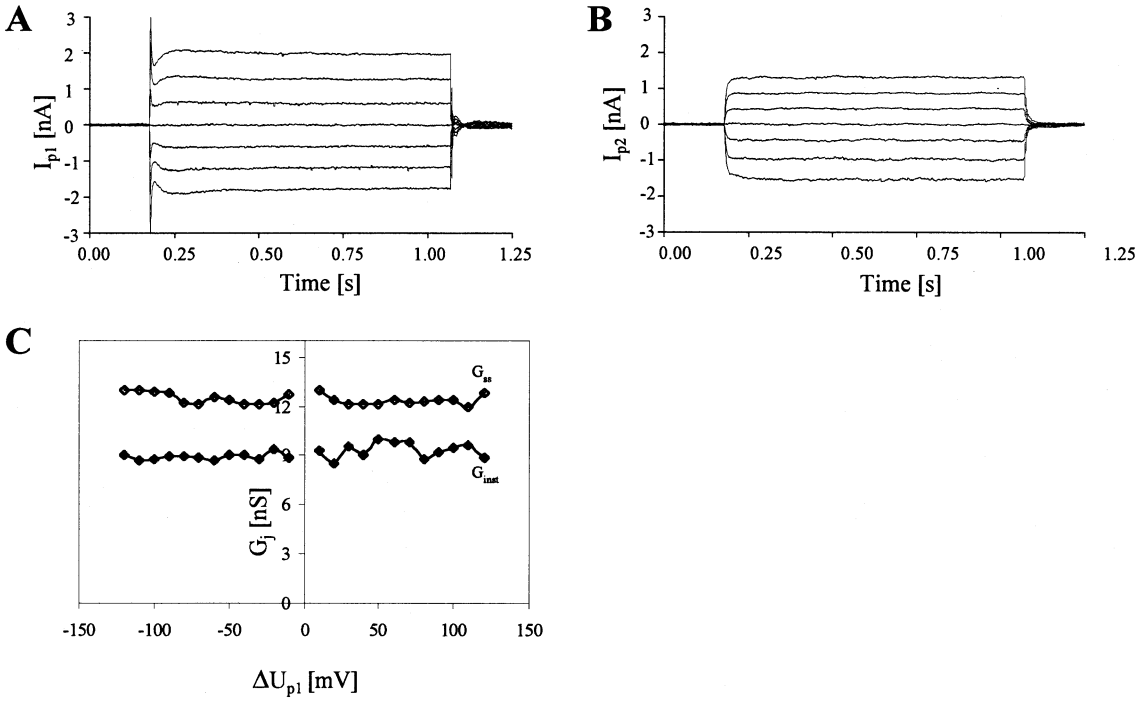

Fig. 4. Evoked currents and corresponding gap junctional conductance. (*A* and *B*) Current responses of electrode/pipette 1 and 2 after application of the voltage protocol given in Fig. 2*A*, *B*. (*C*) G_{inst} and G_{ss} as function of ΔU_{p1}. For further explanation, *see* Fig. 2 and text.

determined after whole-cell formation (Fig. 5*D*). The cell shrinkage started 2–3 min after whole-cell formation and was followed for about 10 min. The cell diameter of the cells decreased by about 75% within 10 min. Thereafter further morphological changes of the cells, like bleb formation, were observed. Occasionally (*data not shown*), an increase of the cell volume was observed within 1–2 min after establishing the whole-cell configuration, which was followed by the described cell shrinkage.

Ca^{2+}-free Bath and Pipette Solution A

To analyze an involvement of Ca^{2+} influx in the observed cellular processes initiated by whole-cell formation with pipette solution A (*see* Fig. 5), the experiments were repeated in nominally Ca^{2+}-free bath containing 10 mM EGTA. Fig. 6 presents a typical experiment. Fig. 6*A* shows a significant, but transient rise of $[Ca^{2+}]_i$ for 2–3 min in both cells, which is induced by the whole-cell formation. Gap junctional conductance G_j (Fig. 6*B*) as well as cell volume (Fig. 6*C*) appear to be unchanged during the time span of an experiment of up to 30 min. These data indicate an involvement of Ca^{2+} in the observed changes in cell morphology and G_j (*compare* Fig. 5*B*,*C* and Fig. 6*B*,*C*).

Control Bath and Pipette Solution Containing Cs^+

Since it is known that an increase of $[Ca^{2+}]_i$ amplifies a Ca^{2+}-dependent K^+ efflux, the influence of the latter was investigated. A K^+ efflux was blocked by addition of 40 mM Cs^+ to the pipette solution (pipette solution B, Table 1). The time course of the three measured cellular parameters is presented in Fig. 7. Again a transient rise of $[Ca^{2+}]_i$ was observed for the two adjacent cells (Fig. 7*A*). It is interesting that the transient change of $[Ca^{2+}]_i$ in one cell caused no visible change of $[Ca^{2+}]_i$ in the adjacent coupled cell. G_j (Fig. 7*B*) as well as the cell volume (Fig. 7*C*) stayed constant throughout the measuring time of an hour. Comparison of Figs. 6 and 7 indicates that the behavior of $[Ca^{2+}]_i$, cell morphology and G_j after whole-cell formation under blockade of K^+ efflux by Cs^+ is comparable with that observed in Ca^{2+}-free bath solution.

Control Bath and Pipette Solution A Containing 8-Br-cGMP

The data presented in Figs. 5, 6 and 7 indicate that whole-cell formation generates a Ca^{2+}-dependent K^+ efflux that is related to gap junctional uncoupling. Since it can be assumed that by whole-cell formation regulatory molecules are washed out by dialysis against the pipette solution, a corresponding substitute was evaluated. 3′,5′-Cyclic guanosine monophosphate (cGMP) was considered a suitable molecule, since it is known that cGMP controls various cellular functions like regulation of $[Ca^{2+}]_i$ and K^+ efflux. The activation of both ions' fluxes has been related to the early phase of apoptosis (Hirsch et al., 1999; Moreno et al., 2001). 50 μM 8-Br-cGMP,

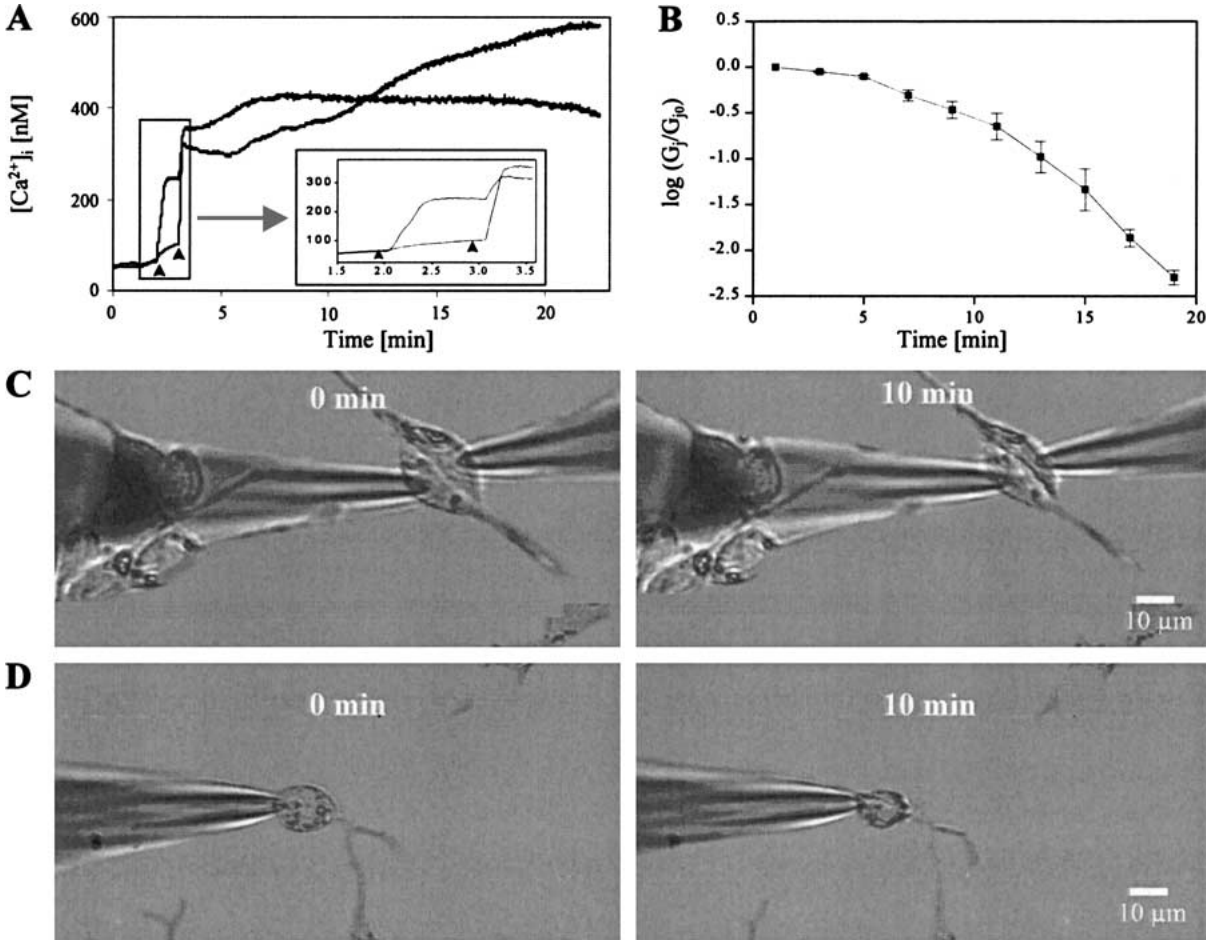

Fig. 5. Effect of double whole-cell formation on the time course of $[Ca]_i$, gap junctional conductance, and shape of the cell pair in control bath and with pipette solution A (Table 1). (*A*) Time course of $[Ca^{2+}]_i$ after establishing the two consecutive whole-cell configurations, which were started from cell-attached configuration of the two pipettes. After whole-cell formation at the first cell, marked by ▲, a rapid rise of $[Ca^{2+}]_i$ occurs, while $[Ca^{2+}]_i$ in the second cell (*see* lower trace in the inset between the two marks), remains almost unaffected. At the 2nd mark, the whole-cell formation of the second cell is established. The data exhibit a representative experiment of a total of $n = 5$. (*B*) Time course of G_j. For clearer presentation, G_j is normalized to G_{jo} obtained 1 min after double whole-cell formation. The data represent the mean ± SEM of $n = 10$ cell pairs. For the total of 60 experiments, an initial value $G_{jo} = 39.25 \pm 2.37$ nS ($n = 60$) was obtained at $|\Delta U_{p1}| = 10$ mV. (*C*) Shape of a cell pair 0 min and 10 min after double whole-cell formation. (*D*) Shape of a single cell 0 min and 10 min after whole-cell formation. For single cells with an almost spherical form, within 10 min, a reduction of the cell diameter to 77 ± 1.2% ($n = 6$) of the initial value could be estimated.

the non-hydrolyzable form of cGMP, was added to the pipette solution (pipette solution *C*, Table 1). Figure 8 shows that by use of pipette solution *C* the time course of $[Ca^{2+}]_i$, cell volume as well as of G_j was unaffected by whole-cell formation. Also the early transient change of $[Ca^{2+}]_i$, as observed in Figs. 6*A* and 7*A*, was suppressed by the presence of intracellular 8-Br-cMP (Fig. 8*A*). Replacement of cGMP by cAMP up to 0.1 mM did not suppress any of the described cellular responses (*data not shown*).

Discussion

Voltage Dependence of Gap Junctional Coupling

In the GFSHR-17 granulosa cell line variable transjunctional-voltage gating properties were observed (*compare* Figs. 2, 3 and 4). One population showed a bell-shaped behavior of the gap junctional conductance G_j at voltages $|\Delta U_{p1}| \geq 60$ mV (Fig. 3*C*). This property is known for specific connexins forming gap junctional channels. In rat granulosa cells, coexpression of at least two connexins, Cx43 and Cx45, and their concomitant presence within some gap junctional plaques have been demonstrated (Okuma et al., 1996). The simplest configuration is the formation of homotypic channels, which result from the association of homomeric hemichannels or connexons. This configuration can be achieved after expression of connexins in *Xenopus* oocytes or by transfection of connexins in various cell systems. For Cx43 and Cx45 the corresponding homotypic gap junctional channels exhibit a significant voltage dependence (Banach & Weingart, 1996; Steiner &

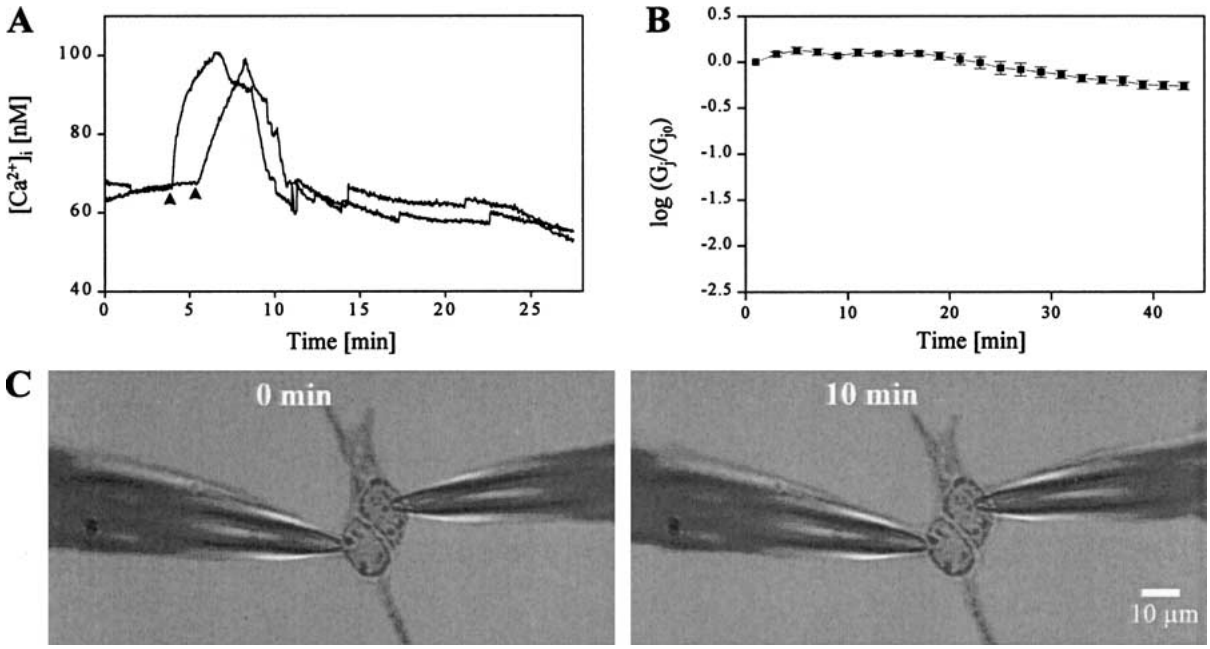

Fig. 6. Effect of double whole-cell formation on the time course of $[Ca^{2+}]_i$, gap junctional conductance, and shape of the cell pair in nominally Ca^{2+}-free control bath containing additionally 10 mM EGTA, and with pipette solution A (Table 1). (*A*) Time course of $[Ca^{2+}]_i$ after establishing the two consecutive whole-cell configurations, which were started from cell-attached configuration of the two pipettes. After whole-cell formation at the first cell, marked by ▲, a rapid rise of $[Ca^{2+}]_i$ occurs, while $[Ca^{2+}]_i$ in the second cell (*see* lower trace between the two marks), remains almost unaffected. At the 2nd mark, the whole-cell formation of the second cell is established. The data show a representative experiment of a total of $n = 5$. (*B*) Time course of G_j. For clearer presentation, G_j is normalized to G_{jo} obtained 1 min after double whole-cell formation. The data represent the mean ± SEM of $n = 5$ cell pairs. (*C*) Shape of a cell pair 0 min and 10 min after double whole-cell formation.

Ebihara, 1996; Stergiopoulos et al., 1999; Elenes et al., 2001), which in the following will be compared with our findings.

The transjunctional voltage-gating properties derived from fitting Eq. 2 to the data of Fig. 3*C* can be compared with the corresponding data obtained for Cx43/Cx43 and Cx45/Cx45 homotypic and Cx43/Cx45 heterotypic gap junctional channels formed in paired *Xenopus* oocytes (Elenes et al., 2001). For homotypic gap junctional channels composed of Cx43 a striking similarity is found for the transjunctional-voltage gating concerning the half-maximal inactivation voltages and the corresponding voltage sensitivities for the transitions between the conductive states. In addition, a similar agreement is found for the corresponding time constants of current inactivation after a transjunctional voltage step (*compare* also Table 2 and Elenes et al., 2001). Such an agreement could be identified for the transjunctional-voltage gating properties of neither Cx45/Cx45 homotypic nor of Cx45/Cx43 heterotypic channels (Elenes et al., 2001). Therefore, it appears likely that the transjunctional-gating properties presented in Fig. 3*C*, which are representative for 15% of a total of 60 experiments, are related to formation of homotypic Cx43/Cx43 gap junctional channels between adjacent granulosa cells. In all the other cases, the steady-state behavior of G_j appears to be voltage-independent. But besides the majority of cell pairs (60%), which showed an ohmic behavior of gap junctional coupling (Fig. 2), two further populations of cell pairs were identified, according to their voltage-dependent response after a voltage step. In these two populations the instantaneous and corresponding steady-state values of G_j differ significantly. One population of cell pairs (5%) showed a gap junctional current or conductance that became activated in a time-dependent but voltage-independent manner (Fig. 4). The other population of cell pairs (15%) exhibited a superimposition of a time-dependent activation and inactivation (*data not shown*).

Variable voltage dependence is known for primary cell systems and has been observed for e.g., coupled Hensen cells of the organ of Corti in the inner ear (Zhao & Santos-Sacchi, 2000; Todt et al., 2001). This variability has been interpreted as a position-related differentiation. In the follicle, granulosa cells are organized in concentric layers. Gap junctional coupling could also vary within the spatial pattern of these cell layers. However, in a cell culture without the necessity of a three-dimensional organization, such a pattern of variable gap junctional coupling is difficult to understand. At the molecular level, the variability in transjunctional voltage-

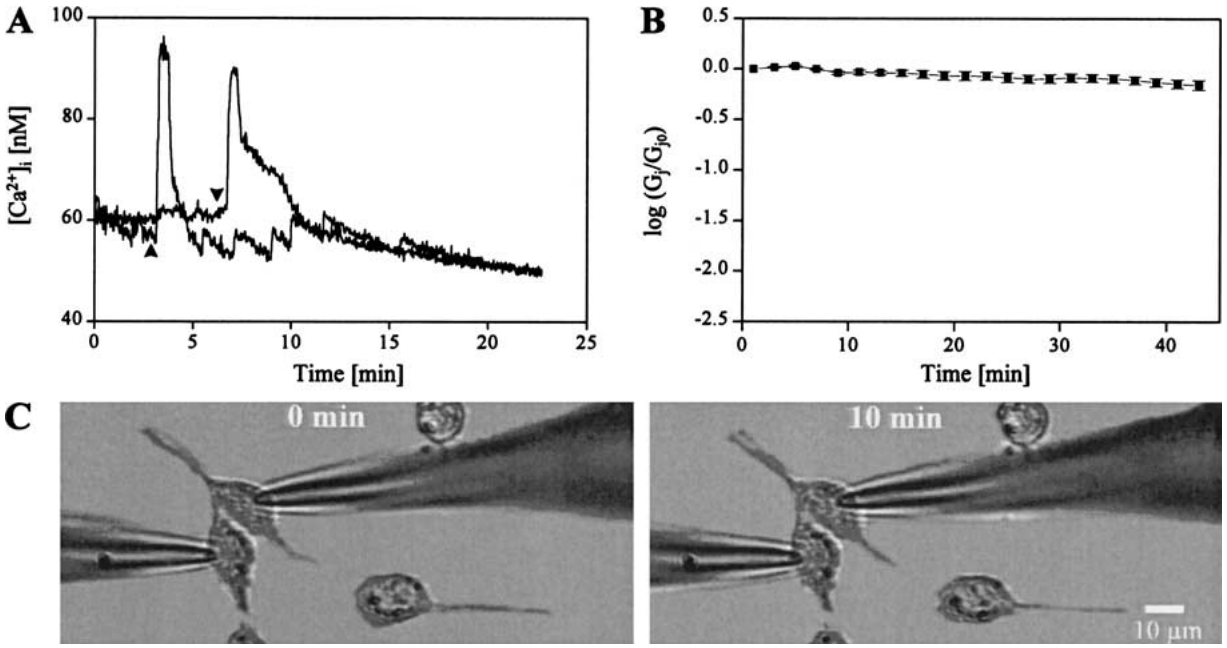

Fig. 7. Effect of double whole-cell formation on the time course of $[Ca^{2+}]_i$, gap junctional conductance, and shape of the cell pair in control bath and with pipette solution B containing Cs^+ (Table 1). (*A*) Time course of $[Ca^{2+}]_i$ after establishing the two consecutive whole-cell configurations, which were started from cell-attached configuration of the two pipettes. After whole-cell formation at the first cell, marked by ▲, a rapid rise of $[Ca^{2+}]_i$ occurs, while $[Ca^{2+}]_i$ in the second cell (*see* upper trace between the two marks), remains almost unaffected. At the 2nd mark, the whole-cell formation of the second cell is established. The data give a representative experiment of a total of $n = 5$. (*B*) Time course of G_j. For clearer presentation, G_j is normalized to G_{jo} obtained 1 min after double whole-cell formation. The data represent the mean ± SEM of $n = 5$ cell pairs. (*C*) Shape of a cell pair 0 min and 10 min after double whole-cell formation.

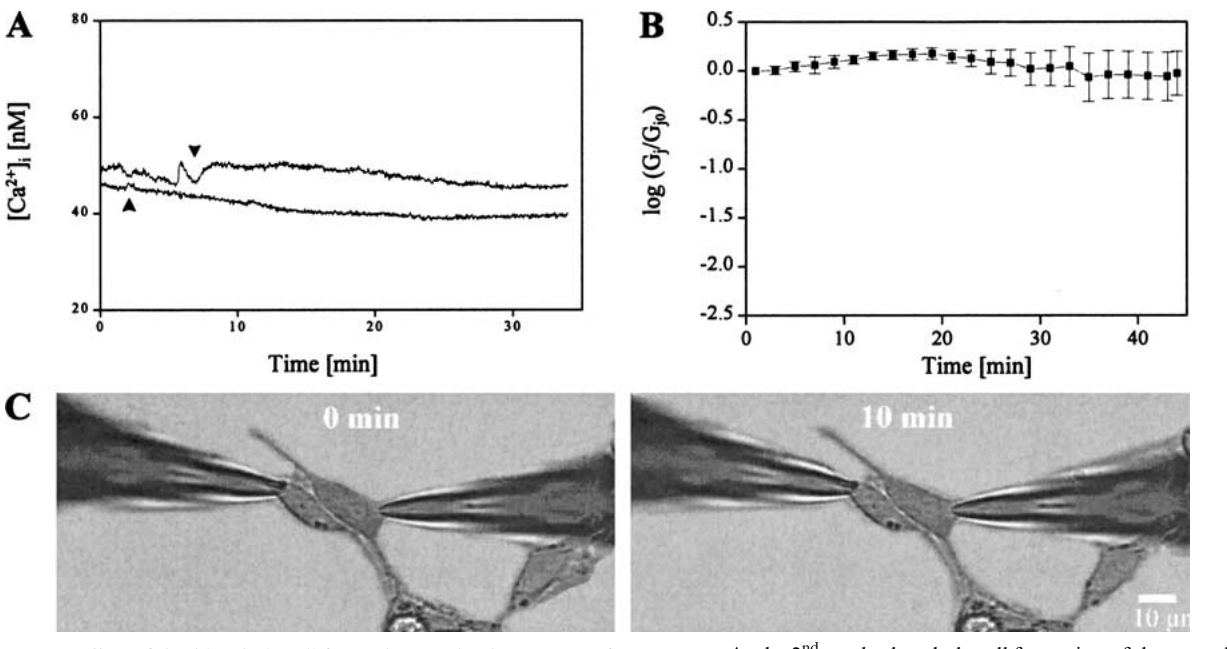

Fig. 8. Effect of double whole-cell formation on the time course of $[Ca^{2+}]_i$, gap junctional conductance, and shape of the cell pair at control bath and pipette solution C containing 5 µM 8-Br-cGMP (Table 1). (*A*) Time course of $[Ca^{2+}]_i$ after establishing the two consecutive whole-cell configurations, which were started from cell-attached configuration of the two pipettes. After whole-cell formation at the first cell, marked by ▲, no significant rise of $[Ca^{2+}]_i$ occurs. At the 2nd mark, the whole-cell formation of the second cell is established. Again the whole-cell formation does not induce an elevation of $[Ca^{2+}]_i$. The data are a representative experiment of a total of $n = 5$. (*B*) Time course of G_j. For clearer presentation, G_j is normalized to G_{jo} obtained 1 min after double whole-cell formation. The data represent the mean ± SEM of $n = 5$ cell pairs. (*C*) Shape of a cell pair 0 min and 10 min after double whole-cell formation.

dependent channel gating has been associated with the coexpression of different connexin types, which form homotypic, heterotypic and heteromeric gap junctional channels (Sosinsky; 1995; White & Bruzzone, 1996; Harris, 2001). Furthermore, post-translational modifications like phosphorylation have also been related to variations in voltage-dependent gating of gap junctional channels (Godwin et al., 1993; Ngezahayo et al., 1998). These modifications of connexins are dynamic processes that can be modulated by the metabolic and the developmental state of the cells (Kanemitsu, Jiang & Eckhart, 1998). It can be speculated that Cx45 assembles with Cx43 to form heteromeric channels whose voltage dependence varies depending on the stoichiometry and post-translational modification of the connexins. Since posttranslational modifications of the connexins may reflect developmental state of the cells (Sommersberg et al., 2000), further studies, including with synchronized GFSHR-17 cells, are necessary to elucidate gap junctional coupling of granulosa cells as a function of cell cycle.

Effect of Whole-cell Formation on $[Ca^{2+}]_i$ and Gap Junctional Coupling

With control bath and absence of cGMP in the pipette solution (Solution A, Table 1), the formation of whole-cell configuration caused several significant cellular changes: a sustained increase in $[Ca^{2+}]_i$ (Fig. 5*A*) that reached the maximal level within less than 3 minutes; cell shrinkage within 2–4 minutes after whole-cell formation, which was completed after about 5 minutes. Within this phase, the cell diameter decreased by about 25% (Fig. 5*B*). Thereafter gap junctional coupling decreased significantly to less than 1% of the starting value within 15 minutes (Fig. 5*C*). It is interesting that this spontaneous gap junctional uncoupling by use of a pure electrolyte as pipette solution was not affected by addition of cAMP. The addition of this cyclic nucleotide had been found to be essential for stable gap junctional coupling during double whole-cell configuration in other cells, like pancreatic acinar cells (Somogyi, Batzer & Kolb, 1989).

The observed cellular changes could be suppressed if the whole-cell configuration was established using a pipette solution containing Cs^+ (Fig. 7; Table 1, Solution *B*) or if Ca^{2+} in the extracellular solution was chelated by EGTA (Fig. 6). However, even use of a pipette solution containing Cs^+ or Ca^{2+}-free extracellular solution did not suppress the generation of a Ca^{2+} spike (Figs. 7*B* and 6*A*) by formation of whole-cell configuration. Surprisingly, the time course and amplitude of the Ca^{2+} increase differed for the two cells of a coupled pair during the consecutive formation of the corresponding whole-cell configuration. At the first whole-cell formation a steep and significant rise in $[Ca^{2+}]_i$ was registered, but only a slow and minor response of $[Ca^{2+}]_i$ could be observed in the neighboring cell, while the second pipette was still being kept in the cell-attached configuration (Fig. 5*A*). Since the two cells are coupled by gap junctional channels, it should be expected that Ca^{2+} diffuses from one cell into the other, so that the $[Ca^{2+}]_i$ response should be of similar amplitude in both cells. Fig. 5*B* could indicate that Ca^{2+} either does not diffuse freely into the neighbouring cell or becomes rapidly stored in intracellular compartments. Lack of visible diffusion is not surprising since it is known that gap junctions are differently permeable to ions and small molecules (Veenestra et al., 1994; White & Paul, 1999). But it should be noted that whole-cell formation of the 2nd cell again caused a significant rise of $[Ca^{2+}]_i$ in this cell, which in this case partially was accompanied by an increase in the first cell. Such an asymmetric response of the two cells to whole-cell formation with pipette solution A was recorded in all investigated cell pairs ($n = 10$).

The induced pronounced Ca^{2+} spike by whole-cell formation is probably caused by washout of regulatory molecules like cGMP (*see* below), which induces a Ca^{2+} release from intracellular Ca^{2+} stores. Therefore, it is assumed that washout of cGMP, but not of cAMP, by the control pipette solution induces a Ca^{2+} release from intracellular stores, which activates a sustained Ca^{2+} influx and Ca^{2+}-dependent K^+ efflux. The activation of these ion fluxes is followed by volume shrinkage and gap junctional uncoupling. Presence of cGMP could directly regulate a K^+ efflux, since a cGMP-dependent inhibition of K^+ channels has been observed in immortalized human kidney epithelial cells (Hirsch et al., 1999). The question arises whether a cGMP-dependent activation of protein kinase, PKG, known for phosphorylation of Cx43, is the key mechanism in gating gap junctional coupling of GFSHR-17 cells. But the observed stable coupling after washout of cGMP when K^+ efflux or Ca^{2+} influx was inhibited seems to indicate the involvement of further gating mechanisms not related to cGMP-dependent connexin phosphorylation or Ca^{2+}-dependent closure of gap junctional channels. Gap junctional uncoupling by altering the osmolarities of extracellular solutions or pipette pressure have been observed in some cell systems like pancreatic acinar cells (Ngezahayo & Kolb, 1990) and supporting cells in Corti's organ (Zhao & Santos-Sacchi, 1998), but in the presented experiments, morphological changes were not generated by changing the membrane tension.

Interestingly, increase of $[Ca^{2+}]_i$ and a Ca^{2+}-dependent K^+ efflux have been demonstrated to serve as a trigger for cell shrinkage and caspase activation, which are major characteristics of apoptosis/necrosis (Dallaporta et al., 1998; Bortner and

Cidlowski, 1999; Gomez-Angelats, Bortner & Cidlowski, 2000; Maeno et al., 2000; Krick et al., 2001). Thus, the whole-cell formation at control pipette solution could induce apoptotic/necrotic processes, e.g., activation of caspase and other proteases that break down the cytoskeletal system, and thereby mediates a decrease of gap junctional communication. This assumption is supported by the finding that 30–60 min after gap junctional uncoupling the whole-cell configuration induced formation of blebs (*data not shown*) similar to apoptotic bodies.

Addition of cGMP to the control pipette solution resulted in unchanged morphological cell shape, the absence of a significant change of $[Ca^{2+}]_i$ and stable gap junctional coupling (Fig. 8). cGMP is one of the messenger molecules known to diffuse through gap junctional channels (Bevans et al., 1998), whose expression is ubiquitous and which regulates different cellular functions like K^+ efflux (Hirsch et al., 1999) and apoptosis (McGee et al., 1997; Estévez et al., 1998). There are several lines of evidence that loss of cytoplasmic K^+ is responsible for cell shrinkage and that it also is a major characteristic of apopotosis (Bortner, Hughes & Cidlowski, 1997; Bortner & Cidlowski, 1999), especially in granulosa cells (Perez et al., 2000). An anti-apoptotic effect of cGMP has been reported in cultured astrocytes (Takuma et al., 2001). In granulosa cells, cGMP is synthesized during the follicular development (Gutkowska et al., 1999; Noubani, Farookhi & Gutkowska, 2000). To account for the presented results, we postulate that whole-cell formation in the absence of cGMP in the pipette solution reduces intracellular cGMP concentration. Depletion of cGMP causes liberation of Ca^{2+} from intracellular stores, a Ca^{2+} influx and promotion of a Ca^{2+}-dependent K^+ efflux. We propose that superposition of these ion fluxes leads to volume shrinkage, disruption of the cytoskeleton and thereby, by an unknown mechanism, to gap junctional uncoupling.

The authors thank Dr. B. Sommersberg, Dr. A. Mayerhofer, Anatomisches Institut, Technische Universität München, Germany, and Dr. A. Amsterdam, Weizman Institute Rehevot, Israel, for providing the GFSHR-17 cell line. The work was partly supported by a grant of the Fritz Thyssen-Stiftung.

References

Ackert, C.L., Gittens, J.E.I., O'Brien, M.J., Eppig, J.J., Kidder, G.M., 2001. Intercellular communication via connexin43 gap junctions is required for ovarian folliculogenesis in the mouse. *Dev. Biol.* **233:**248–270

Banach, K., Weingart, R., 1996. Connexin43 gap junctions exhibit asymmetrical gating properties. *Pfluegers Arch.* **431:**775–785

Bevans, C.G., Kordel, M., Rhee, S.K., Harris, A.L. 1998. Isoform composition of connexin channels determines selectivity among second messengers and uncharged molecules. *J. Biol. Chem.* **273:**2808–2816

Bortner, C.D., Hughes, Jr. A.F.M., Cidlowski, J.A. 1997. primary role for K^+ and Na^+ efflux in the activation of apoptosis. *J. Biol. Chem.* **272:**32436–32442

Bortner, C.D., Cidlowski, J.A. 1999. Caspase independent/dependent regulation of K^+, cell shrinkage, and mitochondrial membrane potential during lymphocyte apoptosis. *J. Biol. Chem.* **274:**21953–21962

Bruzzone, R., White, T.W., Paul, D.L. 1996. Connections with connexins: the molecular basis of direct intercellular signaling. *Eur. J. Biochem.* **238:**1–27

Chen-Izu, Y., Moreno, A.P., Spangler, R.A. 2001. Opposing gates model for voltage gating of gap junctional channels. *Am. J. Physiol.* **281:**C1604–C1613

Dallaporta, B., Hirsch, T., Susin, S.A., Zamzami, N., Larochette, N., Brenner, C., Marzo, I., Kroemer, G. 1998. Potassium leakage during the apoptotic degradation phase. *J. Immunol.* **160:**5605–5615

Elenes, S., Martinez, A.D., Delmar, M., Beyer, E.C., Moreno, A.P. 2001. Heterotypic docking of Cx43 and Cx45 connexons blocks fast voltage gating of Cx43. *Biophys. J.* **81:**1406–1418

Estévez, A.G., Spear, N., Thompson, J.A., Cornwell, T.L., Radi, R., Barbeito, L., Beckman, J.S. 1998. Nitric oxide-dependent production of cGMP supports the survival of rat embryonic motor neurons cultured with brain-derived neurotrophic factor. *J. Neurosci.* **18:**3708–3714

Godwin, A.J., Green, L.M., Walsh, M.P., McDonald, J.R., Walsh, D.A., Fletcher, W.H. 1993. In situ regulation of cell-cell communication by the cAMP-dependent protein kinase and protein kinase C. *Mol. Cell Biochem.* **127-128:**293–307

Gómez-Angelats, M., Bortner, C.D., Cidlowski, J.A. 2000. Cell volume regulation in immune cell apoptosis. *Cell Tissue Res.* **301:**33–42

Goodenough, D.A., Simon, A.M., Paul, D.L. 1999. Gap junctional intercellular communication in the mouse ovarian follicle. *In:* Gap junction-mediated intercellular signalling in health and disease. Novartis foundation, Cardew, editor, pp. 226–240 John Wiley & Sons, Chichester, New York, Weinheim, Brisbane, Toronto, Singapore

Grynkiewicz, G., Poenie, M., Tsien, R.Y. 1985. A new generation of Ca^{2+} indicators with greatly improved fluorescence properties. *J. Biol. Chem.* **260:**3440–50

Gutkowska, J., Jankowski, M., Sairam, M.R., Fujio, N., Reis, A.M., Mukaddam-Daher, S., Tremblay, J. 1999. Hormonal regulation of natriuretic peptide system during induced follicular development in the rat. *Biol. Repr.* **61:**162–170

Harris, A.L. 2001. Emerging issues of connexin channels: biophysics fills the gap. *Q. Rev. Biophys.* **34:**325–472

Hirsch, J.R., Weber, G., Kleta, L., Schlatter, E. 1999. A novel cGMP-regulated K^+ channel in immortalized human kidney epithelial cell (IHKE-1). *J. Physiol.* **519:**645–655

Kanemitsu, M.Y., Jiang, W., Eckhart, W. 1998. Cdc2-mediated phosphorylation of the gap junction protein, connexin43, during mitosis. *Cell Growth Differ.* **9:**13–21

Keren, T.I, Dantes, A., Sprengel, R., Amsterdam, A. 1993. Establishment of steroidegenic granulosa cell lines expressing follicle stimulating hormone receptors. *Mol. Cell Endocrinol.* **95:**R1–R10

Krick, S., Platoshyn, O., Sweeney, M., Kim, H., Yuan, J.X.-J. 2001. Activation of K^+ channels induces apoptosis in vascular smooth muscle cells. *Am. J. Physiol.* **280:**C970–C979

Maeno, E., Ishizaki, Y., Kanazeki, T., Hazama, A., Okada, Y. 2000. Normotonic cell shrinkage because of disordered volume regulation is an early prerequisite to apoptosis. *Proc. Natl. Acad. Sci. USA* **97:**9487–9492

McGee, E., Spears, N., Minami, S., Hsu, S.-Y., Chung, Y.-Y., Billig, H., Hsueh, A.J.W. 1997. Preantral ovarian follicles in

serum-free culture: suppression of apoptosis after activation of cyclic guanosine 3′,5′-moonophosphate pathway and stimulation of growth and differentiation by follicle-stimulating hormone. *Endocrinology* **138:**2417–2424

Moreno, H., Vega-Saena de Miera, E., Nadal, M.S., Amarillo, Y., Rody, B. 2001. Modulation of Kv3 potassium channels expressed in CHO cells by a nitric oxide-activated phosphatase. *J. Physiol.* **530:**345–358.

Neyton, J., Trautmann, A. 1985. Single-channel currents of an intercellular junction. *Nature* **317:**331–335

Ngezahayo, A., Kolb, H.-A. 1990. Gap junctional permeability is affected by volume changes and modulates volume regulation. *FEBS Lett.* **276:**6–8

Ngezahayo, A., Kolb, H.-A. 1994. Regulation of gap junctional coupling in isolated pancreatic acinar cell pairs by cholecystokinin-octapeptide, vasoactive intestinal peptide (VIP) and a VIP-antagonist. *J. Membrane Biol.* **139:**127–136

Ngezahayo, A., Zeilinger, C., Todt, L., Marten, I., Kolb, H.-A. 1998. Inactivattion of expressed and conducting rCx46 hemichannels by phosphorylation. *Pfluegers Arch.* **436:**627–629

Noubani, A., Farookhi, R., Gutkowska, J. 2000. B-type natriuretic peptide receptor expression and activity are hormonally regulated in rat ovarian cells. *Endocrinology* **141:**551–559

Okuma, A., Kuraoka, A., Iida, H., Inai, T., Wasano, K., Shibata, Y. 1996. Colocalization of connexin 43 and connexin 45 but absence of connexin 40 in granulosa cell gap junctions of rat ovary. *J. Reprod. Fert.* **107:**255–264

Perez G.I., Maravei, D.V., Trbovich, A.M., Cidlowski, J.A., Tilly, J.L., Hughes Jr. F.M., 2000. Identification of potassium-dependent and -independent components of the apoptotic machinery in mouse ovarian germ cells and granulosa cells. *Biol. Reprod.* **63:**1358–1369

Schreiber, J.R., Beckmann, M.W., Polacek, D., Davis, P.F. 1993. Changes in gap junction connexin-43 messenger ribonucleic acid levels associated with rat follicular development as demonstrated by in situ hybridization. *Am. J. Obstet. Gynecol.* **168:**1094–2204

Sommersberg, B., Bulling, A., Salzer, U., Frohlich, U., Garfield, R.E., Amsterdam, A., Mayerhofer, A. 2000. Gap junction communication and connexin 43 gene expression in a rat granulosa cell line: regulation by follicle-stimulating hormone. *Biol. Reprod.* **63:**1661–1668

Somogyi, R., Batzer, A., Kolb, H.-A. 1989. Inhibition of electrical coupling in pairs of murine pancreatic acinar cells by OAG and isolated protein kinase C. *J. Membrane Biol.* **108:**273–282

Sosinsky, G. 1995. Mixing of connexins in gap junction membrane channels. *Proc. Natl. Acad. Sci. USA* **92:**9210–9214

Steiner, E., Ebihara, L. 1996. Functional characterization of canine connexin45. *J. Membrane Biol.* **150:**153–161

Stergiopoulos, K., Alvarado, J.L., Mastroianni, M., Ek-Vitorin, J.F., Taffet, S.M., Delmar, M. 1999. Hetero-domain interactions as a mechanism for the regulation of connexin channels. *Circ. Res.* **84:**1144–1155

Takuma, K., Phuagphong, P., Lee, E., Mori, K., Baba, A., Matsuda, T. 2001. Anti-apoptotic effect of cGMP in cultured astrocytes. *J. Biol. Chem.* **276:**48093–48099

Tilly, J.L. 1996. Apoptosis in ovarian function. *Rev. Reprod.* **1:**162–172

Todt, I., Ngezahayo, A., Ernst, A., Kolb, H.-A. 2001. Hydrogen peroxide inhibits gap junctional coupling and modulates intracellular free calcium in cochlear Hensen cells. *J. Membrane Biol.* **181:**107–114

Veenstra, R. 2001. Voltage clamp limitations of dual whole-cell gap junction current and voltage recordings. I. Conductance measurements. *Biophys. J.* **80:**2231–2247

Veenstra, R.D., Wang, H.Z., Beyer, E.C., Brink, P.R. 1994. Selective dye and ionic permeability of gap junction channels formed by connexin45. *Circ. Res.* **75:**483–489

White T.W., Bruzzone, R. 1996. Multiple connexin proteins in single intercellular channels: connexin compatibility and functional consequences. *J. Bioenerg. Biomembr.* **28:**339–350

White, T.W., Paul, D.L. 1999. Genetic diseases and gene knockouts reveal diverse connexin functions. *Annu. Rev. Physiol.* **61:**283–310

Wiesen, J.F., Midgley, R.A. 1994. Expression of connexin43 gap junction messenger ribonucleic acid and protein during follicular atresia. *Biol. Reprod.* **50:**336–348

Willecke, K., Eiberger, J., Degen, J., Eckardt, D., Romualdi, A., Guldenagel, M., Deutsch, U., Sohl, G. 2002. Structural and functional diversity of connexin genes in the mouse and human genome. *Biol. Chem.* **383:**725–737

Wright, C.S., Becker, D.L., Lin, J.S., Warner, A.E., Hardy, K. 2001. Stage-specific and differential expression of gap junctions in the mouse ovary: connexin-specific roles in follicular regulation. *Reproduction* **121:**77–88

Zhao, H.B., Santos-Sacchi, J. 1998. Effect of membrane tension on gap junctional conductance of supporting cells in Corti's Organ. *J. Gen. Physiol.* **112:**447–455

Zhao, H.B., Santos-Sacchi, J. 2000. Voltage gating of gap junctions in cochlear supporting cells: evidence for nonhomotypic channels. *J. Membrane Biol.* **175:**17–24